PHYSICAL REVIEW D

PARTICLES AND FIELDS

THIRD SERIES, VOLUME 40, NUMBER 3 1 AUGUST 1989

The $K_S^0K_S^0\pi^0$ system produced in π^-p interactions at 21.4 GeV/c

M. G. Rath,[a,*] N. M. Cason,[a] J. R. Bensinger,[b] J. M. Bishop,[a] N. N. Biswas,[a] J. K. Busenitz,[a] A. Etkin,[c] K. J. Foley,[c] M. R. Fortner,[b,†] L. R. Fortney,[f] J. Goo,[e] V. P. Kenney,[a] L. E. Kirsch,[b] M. A. Kramer,[e] S. J. Lindenbaum,[d] R. S. Longacre,[c] W. A. Love,[c] E. McCrory,[f,‡] T. W. Morris,[c] H. Piekarz,[b,§] J. Piekarz,[a] E. D. Platner,[c] R. A. Poster,[b,**] R. C. Ruchti,[a] A. C. Saulys,[c] W. D. Shephard,[a] and P. Zogrofou[b]

[a]*University of Notre Dame, Notre Dame, Indiana 46556*

[b]*Brandeis University, Waltham, Massachusetts 02254*

[c]*Brookhaven National Laboratory, Upton, New York 11973*

[d]*Brookhaven National Laboratory, Upton, New York 11973 and City College of New York, New York, New York 10031*

[e]*City College of New York, New York, New York 10031*

[f]*Duke University, Durham, North Carolina 27706*

(Received 13 February 1989)

The $K_S^0K_S^0\pi^0$ systems, a pure $C=+1$ state, has been studied in the reaction $\pi^-p\to K_S^0K_S^0\pi^0n$ at 21.4 GeV/c. The $K_S^0K_S^0\pi^0$ spectrum is significantly different from the $K\bar{K}\pi$ distribution observed in other lower-energy peripheral hadroproduction experiments. In addition to production of the $f_1(1285)$, evidence for production of the $\eta(1460)$ [sometimes called the $\iota(1460)$] based on mass spectra and a Dalitz-plot spin-parity analysis is reported. The narrower, lower-mass state observed in other $K\bar{K}\pi$ experiments is observed weakly if at all in this experiment. Hadronic production of the $\eta(1460)$, which is a good glueball candidate because of its presence in J/ψ radiative decay, suggests possible mixing with the $q\bar{q}$ sector.

I. INTRODUCTION

There is now good evidence that there are at least six isoscalar states coupling to the $K\bar{K}\pi$ decay channel in the region from 1280 to 1530 MeV/c^2. These states are the $\eta(1280)$, the $f_1(1285)$, the $\eta(1420)$, the $f_1(1420)$ (commonly referred to as the E meson), the $\eta(1460)$ [commonly referred to as the $\iota(1460)$], and the $f_1'(1530)$. It would appear that in both the pseudoscalar and in the axial-vector sectors, more states are present than can be accommodated by the simple $q\bar{q}$ model and that exotic states containing constituent gluons or four quarks must be present. The present experiment is designed to study these states in order to clarify their nature.

We shall briefly summarize the evidence for, and the properties of these states as observed in peripheral and central hadroproduction, in J/ψ radiative and hadronic decay, in $\gamma\gamma$ interactions, and in $\bar{p}p$ annihilation before describing the results of the present experiment.

A. The $J^{PC}=1^{++}$ (axial-vector) states

The $f_1(1285)$ is a well-known state with $J^{PC}=1^{++}$ which has been observed to decay into $K\bar{K}\pi$ (dominantly to $a_0\pi$) and to $\eta\pi\pi$. Its properties have been studied both in peripheral hadroproduction [where it is present in πp (Refs. 1–5) and in $\bar{p}p$ (Ref. 6) interactions but not in Kp interactions] and in central hadroproduction.[7–9] It has also been observed[10] in $\bar{p}p$ annihilation in gaseous hydrogen which enhances P-wave annihilation relative to annihilation in liquid hydrogen. It is an excellent candidate for the nonstrange isoscalar of the axial-vector nonet.

Strong evidence for the $f_1(1420)$ comes from production in central hadroproduction,[8,9] in $\gamma\gamma^*$ interactions,[11–15] and in J/ψ hadronic decays.[16,17] Although one peripheral hadroproduction experiment claims evidence for the state,[2] most such experiments find it present at a very low level if at all. Since it is not produced strongly either in Kp, in πp, or in $\bar{p}p$ peripheral interactions, it is not a good candidate for a $q\bar{q}$ nonet member and hence is more likely a four-quark or hybrid state.

The $f_1'(1530)$ is the best candidate for the isoscalar $s\bar{s}$ member of the axial-vector nonet since it has been observed in peripheral K^-p interactions.[18,19] It is not strongly produced in peripheral πp scattering although some evidence for its production[20] at a low level has been presented which would be indicative of some small mixing with the nonstrange sector.

B. The $J^{PC}=0^{-+}$ (pseudoscalar) states

Since the isoscalar ground-state members of the $q\bar{q}$ pseudoscalar nonet are well known [the $\eta(550)$ and the $\eta'(980)$], states observed at higher mass are expected to be radially excited states if they are ordinary $q\bar{q}$ states. The three isoscalar states which appear to be present in the higher-mass data would constitute an excessive number of candidates for the $N=2$ nonet and would indicate the presence of at least one non-$q\bar{q}$ state.

The $\eta(1280)$ has been observed in the $\eta\pi\pi$ mode in two separate ($\pi^- p$) peripheral hadroproduction experiments.[4,5] There is also some indication of its presence in the $K\bar{K}\pi$ final state.[20] It is thus a good candidate for the nonstrange isoscalar state of the $N=2$ $q\bar{q}$ nonet. On the other hand, the $\eta(1420)$ is clearly seen in both the $\eta\pi\pi$ (Ref. 5) and the $K\bar{K}\pi$ (Ref. 1) modes (also in $\pi^- p$ interactions) and represents a second candidate for the same state. Evidence for this $\eta(1420)$ was originally seen in $\bar{p}p$ annilihilation at rest.[21] Neither the $\eta(1280)$ nor the $\eta(1420)$ are observed in $K^- p$ interactions.

An apparently distinct state from the $\eta(1420)$ is the $\eta(1460)$ which has been observed in J/ψ radiative decay.[22–24] This latter state is observed at a higher mass and with a broader width than the state observed in hadroproduction and is a good candidate for a glueball since the dominant diagram for J/ψ radiative decay includes a coupling to two hard gluons. We are thus left in the 0^{-+} sector with three isoscalars, none of which are good candidates for the $s\bar{s}$ member of the $N=2$ $q\bar{q}$ nonet.

II. DESCRIPTION OF THE EXPERIMENT

This experiment [Brookhaven Alternating Gradient Synchrotron (AGS) experiment 769] is a study of the exclusive reaction

$$\pi^- p \to K_S^0 K_S^0 \pi^0 n$$

at π^- momentum of 21.4 GeV/c. Some results have been previously published.[25,26] The momentum corresponds to a c.m. energy 1.6 times larger than in Ref. 1 or 5. This facilitates the search for new states at higher mass. It is important to note that our higher energy could lead to different combinations of production mechanisms than the lower-energy experiments possibly leading to different production characteristics.

The final state observed in this experiment has the unique advantage that the $K_S^0 K_S^0 \pi^0$ system is an eigenstate of C with $C=+1$. This removes the complication introduced by the presence of $C=-1$ states in the analysis.

The experiment was performed at the Brookhaven National Laboratory AGS, utilizing the high-energy unseparated beam (HEUB). This beam consisted mostly of π^- ($\sim 98\%$) with a small fraction of K^- and $\bar{p}$. The central beam momentum was 21.35 GeV/c, $\sigma=0.26$ GeV/c, with a flux of $(1-2)\times 10^6$ π^-/spill.

The target was a 10-cm-diameter $\times$ 30.5-cm-long cylinder of liquid hydrogen contained in a low-mass Dewar. The final state was required to include only neutral particles. To ensure this and to veto events with neutral pions produced at large angles, the target was surrounded on the sides by a lead-scintillator sandwich veto "box." In addition, a plastic-scintillator veto counter was placed at the downstream end of the target.

Charged-particle tracking and triggering were done with the Brookhaven Multiparticle Spectrometer (MPS) II facility.[27,28] It consists of seven drift chambers and four proportional wire chambers (PWC's) in a uniform 7.5-kG magnetic field (Fig. 1).

A lead-glass hodoscope directly downstream of the MPS magnet (Fig. 1) was used to detect photons from π^0 decay. The hodoscope was an upgraded version of one used in a previous experiment. Many of the construction details are similar to that earlier hodoscope described in Ref. 29.

The hodoscope was constructed of 128 lead-glass blocks of two types: SF2 ($8.9\times 8.9\times 33.0$ cm, 12.0 radiation lengths) and SF5 ($10.0\times 10.0\times 35.0$ cm, 13.8 radiation lengths). The blocks were stacked in a manner which would maximize shower sharing and therefore optimize the position resolution. The center block was removed to allow the beam to pass through the hodoscope unimpeded. A cylindrical (10.2-cm-long $\times$ 7.1-cm-diameter) lead-glass light guide (of matching glass type) and an RCA 4900 photomultiplier tube was attached to each block.

After calibration of each module in a test beam consisting of electrons and muons, the gain of each counter was monitored with a single light-emitting diode (LED) optically coupled to each lead-glass block. In addition to the 128 counters used for data collection, three counters were assembled with an americium source and sodium-iodide scintillator attached to the end of the block opposite the photomultiplier tube. These "reference counters" monitored the stability of the LED output. Further details of the hodoscope as used in the present experiment including more detailed discussion of its calibration and monitoring can be found in Ref. 30.

The trigger was designed to select all-neutral final states containing two charged decay vertices (total charged-track multiplicity of four). In order to satisfy the trigger, event candidates were required to have an identified π^- beam track (from beam-line Čerenkov counters, PWC's, and scintillation hodoscopes) and no signal from the veto counters surrounding the target. Charged multiplicity, as measured by two trigger PWC's located 50 and 190 cm downstream of the target (Fig. 1), was required to be consistent with the decay of a $K_S^0 K_S^0$ system.

III. EVENT RECONSTRUCTION

A good event was required to contain four reconstructed charged tracks. Neutral decay vertices were formed from pairs of oppositely charged tracks. It was required that only one unique combination of two decay vertices be formed. The neutral decaying particle (K_S^0) was

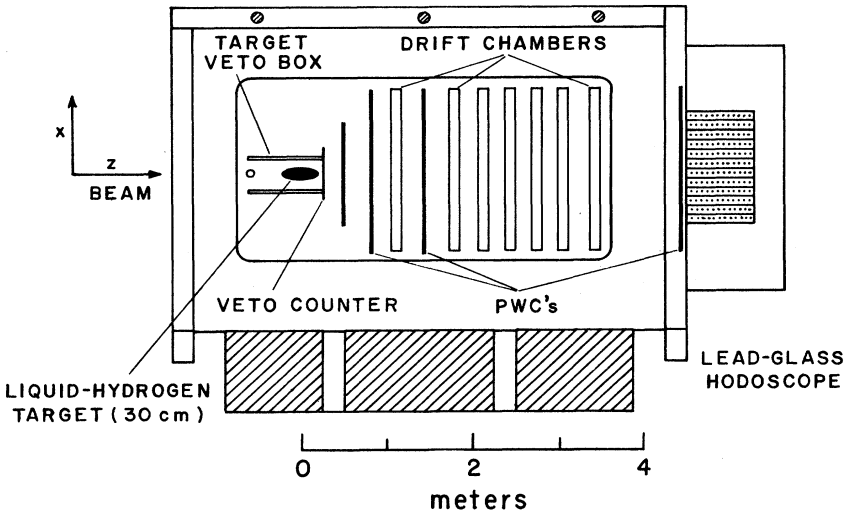

FIG. 1. Schematic of the experiment, showing the MPS II facility and the lead-glass hodoscope.

reeconstructed by combining the momenta of the two charged tracks at the decay vertex. These neutral tracks were extrapolated to find their point of closest approach. If the distance of closest approach was greater than 1 cm the event was rejected. The projection of the incident beam track, reconstructed from the PWC data, was used along with the extrapolated neutral K_S^0 tracks to find the best production vertex point. This point was required to lie within the target volume for the event to be kept.

The effective mass distribution of particles from the decay vertices in which the measured tracks are assumed to be $\pi^+\pi^-$ is shown in Fig. 2(a). The K_S^0 peak observed in this distribution indicates an effective mass resolution of $\sigma=3.0$ MeV/c^2, consistent with the mass resolution quoted for the MPS II (Ref. 27).

The lead-glass hodoscope provides a position and energy measurement for photon candidates. Photon four-vectors are formed by assuming that a π^0 decays at the production vertex. The two-photon effective-mass distribution from the final event sample is shown in Fig. 2(b), showing the π^0 peak with mass of 134.7 MeV/c^2 and full width of 30.7 MeV/c^2. Decays $\eta\rightarrow\gamma\gamma$ were also detected, as seen in the two-photon mass distribution in Fig. 2(c).

For π^0's which have energy greater than 6.5 GeV, the minimum opening angle between the decay photons is such that their separation at the lead-glass hodoscope will be less than 20 cm. With this separation, the photons can enter adjacent lead-glass blocks, and therefore form a single cluster. Events containing a single cluster of energy greater than 6.5 GeV are therefore candidates for "single-center π^0" events.

In order to extract as clean an exclusive $nK_S^0K_S^0\pi^0$ event sample as possible, the events were subjected to multivertex kinematic fits. To minimize fitting time, fits were attempted only for events in which two unique neutral vertices were present; both vertices had decay tracks with effective masses within K_S^0 mass cuts

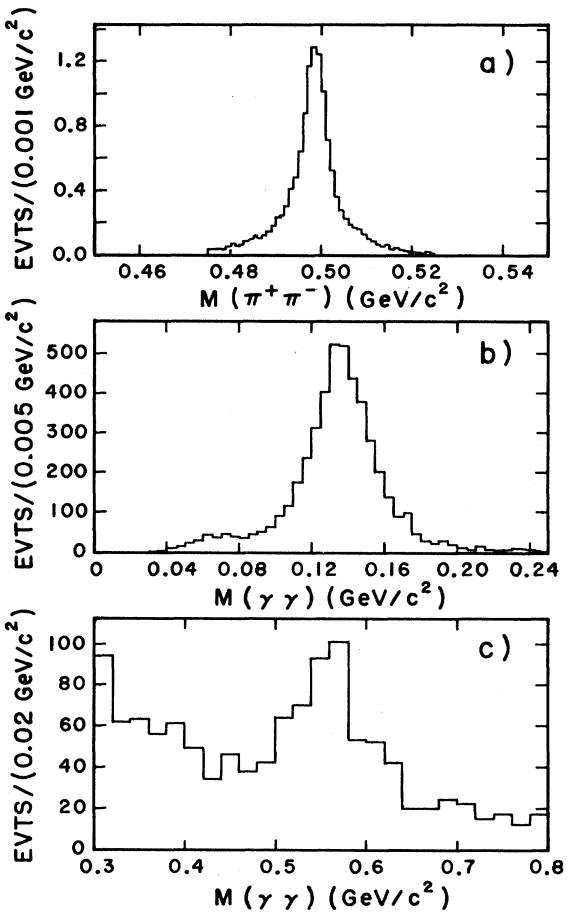

FIG. 2. (a) The $\pi^+\pi^-$ effective-mass distribution for tracks from good decay vertices. (b) and (c) The two-photon effective-mass distribution, showing the (b) π^0 peak and (c) the η peak.

$[475 \leq m(\pi^+\pi^0) \leq 525$ MeV/c^2]; the neutral tracks extrapolated to within 1 cm of each other (good production vertex); and one to four clusters were reconstructed (single-cluster events were required to have $E \geq 5.0$ GeV).

Events were fitted to the hypotheses:

$$(1)\pi^- p \rightarrow K_S^0 K_S^0 \pi^0 n;$$

$$(2)K_S^0 \rightarrow \pi^+\pi^-;$$

and

$$(3)\pi^0 \rightarrow \gamma\gamma \ .$$

This sequence of decays yields eight constraints: three each at the K_S^0 decay vertices, one at the π^0 decay vertex, and one at the production vertex. Single-center π^0 events are fitted to the event hypothesis by assigning the π^0 mass to the cluster. By doing this the π^0 decay constraint is lost, and the fit is made with seven constraints. Events with three or more clusters reconstructed were not included in the analysis of the exclusive channel.

Selections based on unconstrained missing mass were used to increase the purity of the exclusive ($nK_S^0K_S^0\pi^0$) sample. Unconstrained missing-mass-squared (MM^2) distributions from fits to $\pi^- p \rightarrow K_S^0 K_S^0 \pi^0 +$missing mass for the two- [Fig. 3(a)] and one-cluster [Fig. 3(b)] events which gave successful fits to the $\pi^- p \rightarrow K_S^0 K_S^0 \pi^0 n$ hypothesis show the presence of a broad neutron peak and a large background at higher mass. Because of the constraints on the K_S^0 and the π^0 (for two-cluster events), the "background" is still primarily $K_S^0 K_S^0 \pi^0$ events but not the exclusive channel we are isolating.

Likely backgrounds involve events with an extra π^0. Two such states were studied using Monte Carlo techniques.

(1) $\Delta^0 K_S^0 K_S^0 \pi^0$ where $\Delta^0 \rightarrow n\pi^0$. The π^0 from the Δ^0 is typically very low in energy. The photons from this π^0 will generally either miss the lead glass or be below the 300-MeV minimum photon energy.

(2) $nK_S^0K_S^0\pi^0\pi^0$ where both π^0's come from the scattered meson system. Such events contribute to the background when only two photons are reconstructed in the lead glass.

After studies[30] of peripherally produced Monte Carlo events of these types which satisfied normal trigger requirements, fits were made to the experimental missing-mass distributions of Fig. 3. The fits included contributions from the backgrounds listed above parametrized by Gaussian peaks combined with a polynomial. A Gaussian peak for the neutron signal was used. The resultant fits are shown as the solid curves in Fig. 3.

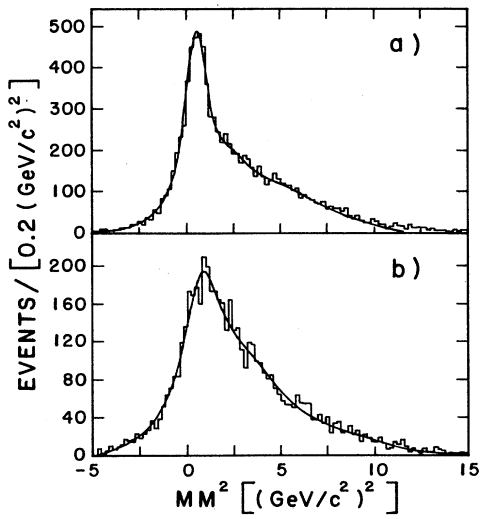

FIG. 3. (a) The missing-mass-squared distribution for events with two photons reconstructed. (b) The missing-mass-squared distribution for single-cluster events. The curves represent fits described in the text.

In both the two- and one-cluster cases the background and signal contributions are approximately equal at about 1.8 GeV^2. A cut was imposed on both data sets requiring -3.0 GeV$^2 \leq MM^2 \leq +1.8$ GeV^2. This yielded samples of 4649 two-cluster events (signal-to-background ratio estimated to be 3.8 to 1) and 1616 single-cluster π^0 events (signal-to-background ratio estimated to be 1.9 to 1). These two samples are combined to provide the final sample of 6265 events used in the analysis which follows. It should again be emphasized that the backgrounds are predominantly real $K_S^0K_S^0\pi^0$ systems.

IV. CHARACTERISTICS OF THE DATA

A. Two-body intermediate states

Three-body final states such as the $K_S^0K_S^0\pi^0$ system under study often decay via intermediate two-body states to the final state observed. Such final states are often described by the isobar model which, in the case of the $K_S^0K_S^0\pi^0$ final state, would involve resonance production in the $K_S^0K_S^0$ and/or the $K_S^0\pi^0$ system.

In the $K_S^0\pi^0$ effective-mass spectrum [Fig. 4(a)], a prominent $K^*(892)$ peak is observed indicating considerable production of the K^*K two-body system (and providing further confirmation of our success in selecting events containing a π^0). This plot has two entries per event. It is not acceptance corrected; the acceptance effects do not significantly affect the resonance structure. The prominence of the K^* peak is enhanced because of the positive C parity of the $K_S^0K_S^0\pi^0$ system: when $C=+1$, as in this system, constructive interference occurs between the two $K_S^0\pi^0$ combinations forming the K^* in the region of overlap of the K^* bands.

The $K_S^0\pi^0$ effective-mass spectrum was fitted with a function including two simple Breit-Wigner resonances and a background of the form

$$a(m - m_{\text{thresh}})^b e^{(-cm - dm^2)} \ , \tag{1}$$

where m is the $K_S^0\pi^0$ mass, m_{thresh} the $K_S^0\pi^0$ threshold mass, and a, b, c, and d, are parameters of the fit (constants). The fit [shown as the smooth curve in Fig. 4(a)] gives a K^* mass of 899.5 ± 1.3 MeV/c^2 and width of 66.9 ± 3.6 MeV/c^2 (including the resolution). The accepted K^* mass is 896.5 ± 0.4 MeV/c^2. The $K_S^0\pi^0$ mass resolution is $\sigma = 26.4\pm8.1$ MeV/c^2 at this mass. Thus the

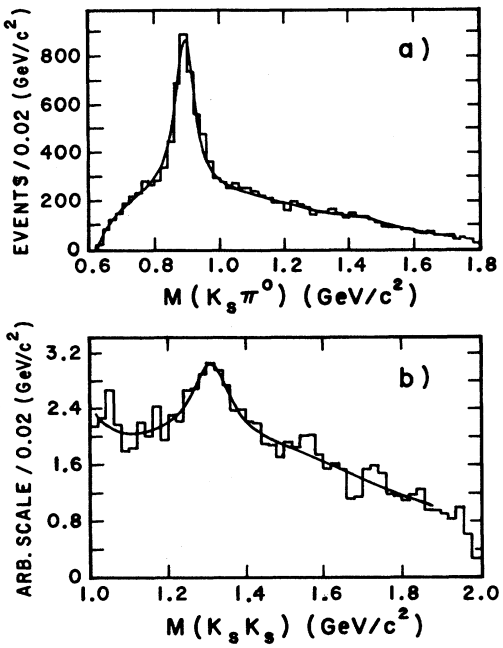

FIG. 4. (a) The $K\pi$ effective-mass spectrum. (b) The acceptance corrected $K_S^0K_S^0$ effective-mass spectrum. The superimposed curves represent fits described in the text.

observed K^* width is consistent with the natural width of 49.9 MeV/c^2.

The second Breit-Wigner contribution has a mass of 1438.6±4.2 MeV/c^2 and width of 88.7±37.2 MeV/c^2. These values are in reasonable agreement with the accepted mass (1423±2 MeV/c^2) and width (99±3 MeV/c^2) of the $K^*(1430)$. The χ_ν^2 of the fit is 1.28 (probability of 8.1%). Fitting the $K_S^0\pi^0$ mass distribution without the second Breit-Wigner contribution gives a χ_ν^2 of 1.48 (probability of 0.8%). Thus although there only appears to be a slight suggestion of a shoulder in the 1400-MeV/c^2 region of the raw data, the structure is consistent with, and does prefer, production of the $K^*(1430)$.

The $K_S^0K_S^0$ effective mass spectrum [Fig. 4(b)] contains peaks at threshold and in the region of 1300 MeV/c^2. The $K_S^0K_S^0$ mass distribution is acceptance corrected. The threshold enhancement indicates the production of a $K\bar{K}$ resonance at or below threshold, such as the $a_0(980)(\delta)$ or the $f_0(975)$. The 1300-MeV region shows evidence of $a_2(1320)$ and/or $f_2(1270)$ production.

The $K_S^0K_S^0$ mass distribution between threshold and 1.9 GeV/c^2 was fitted with a function consisting of a threshold peak parametrized with the coupled-channel resonance form of Flatté,[31] a simple Breit-Wigner resonance, and a sixth-order polynomial. The Flatté parametrization assumed $m_\delta = 983$ MeV/c^2 and coupling strength ratio $g_K/g_\eta = 1.5$.

The Breit-Wigner fit in the region of 1300 MeV gives a mass of 1311.6±7.5 MeV/c^2 and width of 115.4±30.5 MeV/c^2 including the $K_S^0K_S^0$ mass resolution of $\sigma = 5.94\pm2.51$ MeV/c^2. The fit has a χ^2 (per degree of freedom) of 1.42 (probability of 5.3%) over the entire region fitted. Fitting only the region $1.12 \le m(K_S^0K_S^0) \le 1.62$, the same parameters for the peak are found with the fit having a reduced χ^2 of 0.99. Both the mass and the width of the peak are within one standard deviation of the accepted values for the $a_2(1320)$. Performing the same fit but allowing two interfering resonances having the (fixed) parameters of the $a_2(1320)$ and $f_2(1270)$ the a_2 contribution is found to be 2.9±1.8 times greater than that of the f_2. Note that $K_S^0K_S^0\pi^0$ final states with isospin 0 can be produced through the $a_2\pi^0$ intermediate state but the $f_2\pi^0$ state can decay only into $K_S^0K_S^0\pi^0$ systems with isospin 1.

B. The $K_S^0K_S^0\pi^0$ effective-mass spectrum

The $K_S^0K_S^0\pi^0$ effective-mass spectrum is shown in Fig. 5. An enhancement is apparent near 1280 MeV. In the region from 1400 to 1500 MeV (the E region) a broad enhancement appears to be present above a rising background. No significant enhancements are apparent at higher masses.

To investigate the two-body decay channels $a_0\pi^0(\delta\pi^0)$, $a_2\pi^0$, and K^*K, the $K_S^0K_S^0\pi^0$ effective mass distribution is shown with the following cuts:

$$1.26\ \text{GeV}/c^2 \le \text{mass}(K_S^0K_s^0) \le 1.36\ \text{GeV}/c^2 \quad (a_2\ \text{cut}),$$

$$\text{mass}(K_S^0K_s^0) \le 1.08\ \text{GeV}/c^2 \quad (\text{“}\delta\text{” cut}),$$

$$0.84\ \text{GeV}/c^2 \le \text{mass}(K_S^0\pi^0) \le 0.94\ \text{GeV}/c^2 \quad (K^*\ \text{cut}).$$

The $a_2\pi^0$ spectrum [Fig. 6(a)] reveals no statistically significant structure. On the other hand, the $a_0\pi^0$ spectrum [Fig. 6(b)] shows prominent peaks at 1280 MeV/c^2 and near 1450 MeV/c^2. The K^*K spectrum [Fig. 6(c)] produces a sharp rise at threshold which is in the region of the second peak in the $a_0\pi^0$ spectrum. No clear peak is evident in the K^*K spectrum, but it seems likely from this spectrum that K^*K production is present in much of the data in and above the E region.

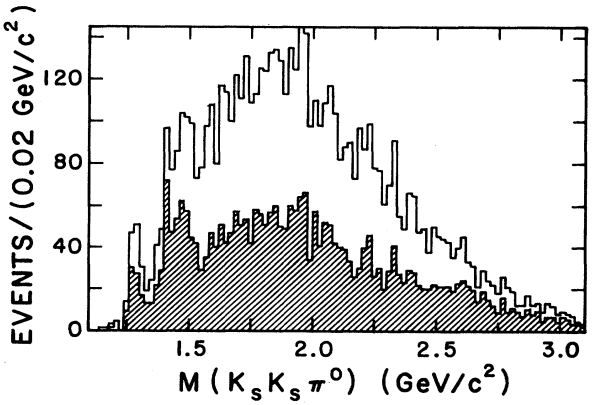

FIG. 5. The $K_S^0K_S^0\pi^0$ effective-mass spectrum for the 6265-event final sample. The shaded area are events with $|t'| > 0.2$ GeV^2.

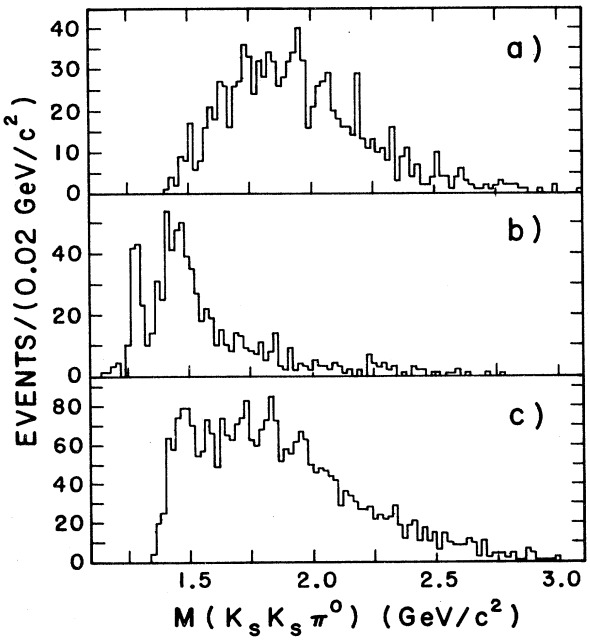

FIG. 6. The $K_S^0K_S^0\pi^0$ effective-mass spectrum for (a) $K_S^0K_S^0$ mass between 1.260 and 1.360 GeV/c^2 (a_2 cut), (b) $K_S^0K_S^0$ mass below 1.08 GeV/c^2 (δ cut), and (c) $K_S^0\pi^0$ mass between 0.84 and 0.94 GeV/c^2 (K^* cut).

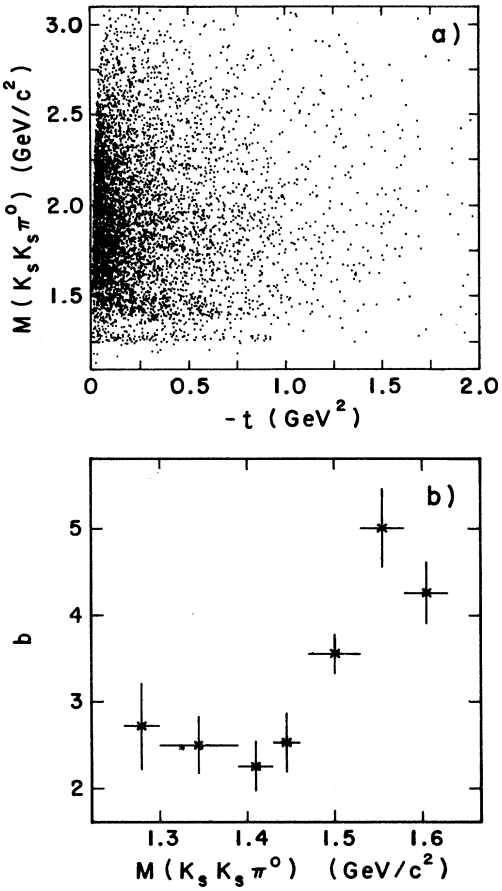

FIG. 7. (a) Scatter plot of the $K_SK_S\pi^0$ effective mass vs the momentum transfer $(-t)$. (b) Plot of the fitted momentum-transfer slope parameter b (see text) as a function of the $K_SK_S\pi^0$ effective mass.

C. Production mechanism

The t distribution for the entire event sample is peaked at low t. In Fig. 7(a) the momentum transfer is shown in a scatter plot versus the $K_S^0K_S^0\pi^0$ mass (a Chew-Low plot). The region below about 1.5 GeV/c^2 has a broader t dependence, with a less pronounced low-t enhancement. The distributions of $t'=|t-t_{\min}|$ have been fitted with exponential functions $f=Ae^{-bt'}$ in successive $K_S^0K_S^0\pi^0$ mass bins up to 1.620 GeV/c^2. Figure 7(b) gives the parameter b as a function of the $K_S^0K_S^0\pi^0$ mass; the horizontal bar on each point gives the extent of the mass bin. It is clear that the lower-mass production [including the $f_1(1285)$ and the E region] has a much broader t' dependence than does the higher-mass production suggesting that the production mechanism is different below 1.5 GeV/c^2 from that above 1.5 GeV/c^2. If the production of the $K_S^0K_S^0\pi^0$ final state is interpreted in terms of single-particle exchange, production in the $f_1(1285)$ and E regions involves exchange of a more massive state—perhaps a_0 or a_2 exchange as opposed to, say, ρ exchange—than production at high $K_S^0K_S^0\pi^0$ effective mass.

The t dependence of Fig. 7 suggests a method of enhancing selection of states produced in a_0 or a_2 exchange. Requiring $-t'>0.2$ GeV^2 preferentially removes events produced with a steeper t dependence. The resulting mass distribution after such a cut for the remaining 2953 events is shown as the shaded region in Fig. 5. The peak in the E region is now more distinct suggesting that much of the background is due to processes with a steeper t dependence.

V. FITS TO THE $K_S^0K_S^0\pi^0$ MASS SPECTRUM

The $K_S^0K_S^0\pi^0$ mass spectrum for events with $-t'>0.2$ GeV^2 was fitted to determine the parameters of the enhancements. The spectrum was fitted with standard Breit-Wigner resonance forms in which the resonance width was modified by the threshold factor $(q/q_0)^{2l+1}$. Here q and q_0 represent the breakup momentum of the $K_S^0K_S^0\pi^0$ system into two bodies (q_0 being the momentum on resonance) and l is the relative angular momentum of the two-body system.

Determination of q and q_0 requires a hypothesis for the decay channel. The $f_1(1285)$ (lower peak) was fitted assuming an ($a_0\pi$, $l=1$) decay. The upper peak was fitted assuming ($a_0\pi$, $l=0$ and 1) and (K^*K, $l=0$ and 1) decays. The fits were also tried without the threshold factors. The fitting function included two or three Breit-Wigner functions, allowing for the possibility that the

broad upper peak could consist of two resonances. Resonance peaks of like spin (J) were allowed to interfere, the relative coherence being a variable of the fit. Each fit also included a background given by Eq. (1), in which m is now the $K_S^0K_S^0\pi^0$ mass and m_{thresh} the $K_SK_S^0\pi^0$ threshold mass. The fits extend to a mass of 2.27 GeV/c^2.

To calculate q and q_0 in K^*K decay, a weighted average of $m(K\pi)$ between threshold and maximum ($m_{K\pi}=M-m_K$) was calculated, in which the weighting function was the Breit-Wigner form [$F_{\text{BW}}(K^*)$] for the K^*:

$$m(K\pi)_{\text{ave}}=\frac{\int_{\text{thresh}}^{\max} m(K\pi)F_{\text{BW}}(K^*)dm(K\pi)}{\int_{\text{thresh}}^{\max} F_{\text{BW}}(K^*)dm(K\pi)} . \quad (2)$$

The $K_S^0K_S^0\pi^0$ mass resolution (between threshold and 2.5 GeV/c^2) was determined from the multivertex fits to be of the form $(\delta m/m)=0.0125\pm0.0083$, or $\sigma=18.1\pm12.0$ MeV/c^2 at a $K_S^0K_S^0\pi^0$ mass of 1450 MeV/c^2. The value reported for the widths of the resonances in each of the fits includes the broadening due to this resolution.

Results for the Breit-Wigner peak in the region of 1280 MeV/c^2 are similar in all of the fits, with mass 1280.1 ± 2.1 MeV/c^2 and width 17.9 ± 10.9 MeV/c^2. These values are consistent with those of the $f_1(1285)$ meson.

In the region between 1400 and 1500 MeV, the single Breit-Wigner fits with $a_0\pi(S)$, $K^*K(S)$, and consistent width all yield, within errors, a fitted mass of 1452.8 ± 6.8 MeV/c^2 and width 99.9 ± 11.4 MeV/c^2. Figure 8(a) shows the fit using a spin-zero $a_0\pi$ (S-wave) Breit-Wigner form for this peak. This fit has a χ^2 per degree of freedom of 1.44 (2.7% probability) over the 55 bins fitted.

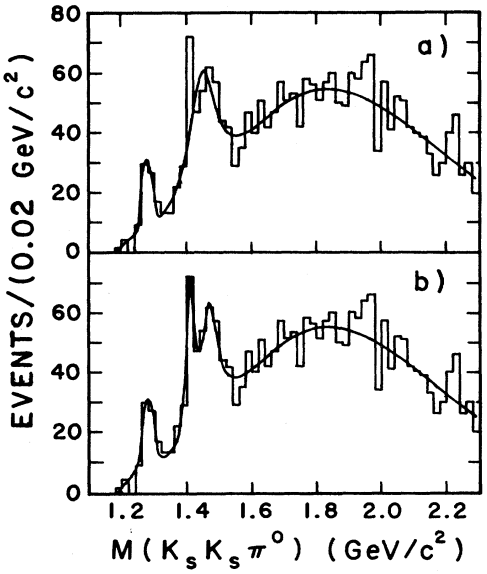

FIG. 8. The $K_SK_S\pi^0$ effective mass-spectrum for events with $-t'>0.2$ GeV^2. (a) The fit with two Breit-Wigner peaks. (b) The fit with three Breit-Wigner peaks.

The relatively poor χ^2 of this fit is largely a result of the bad fit to the bin at 1400–1420 MeV/c^2.

The fit with a single Breit-Wigner peak yields a mass and width consistent with the parameters of the $\iota(1460)$ as seen in radiative J/ψ decay,[22–24] particularly the results reported by the Mark III Collaboration.[24] The ι has been found to be a 0^{-+} state. Identification of the observed peak with it depends on the results of the spin-parity analysis.

Although the statistical significance of the excess of events in the single bin between 1400 and 1420 MeV/c^2 is limited, the best fit to the spectrum is obtained by fitting the E region with two Breit-Wigner functions: a spin-zero $a_0\pi$ resonance of mass 1412.8 ± 5.4 MeV/c^2 and width 19.0 ± 7.0 MeV/c^2, and a spin-zero K^*K resonance of mass 1475.0 ± 3.8 MeV/c^2 and width 50.6 ± 12.7 MeV/c^2. This fit has a $\chi_\nu^2=1.13$ (probability of 22.7%), and is shown in Fig. 8(b). When the higher mass peak is assumed to be a spin-one K^*K resonance, the two peaks are found to have masses of 1412.3 ± 3.6 MeV/c^2 and 1488.0 ± 4.6 MeV/c^2, and widths of 25.4 ± 4.7 MeV/c^2 and 81.6 ± 8.0 MeV/c^2. The resulting χ_ν^2 is 1.11.

The lower peak in the E region has mass and width consistent with those of the $f_1(1420)$ and the $\eta(1420)$ meson. In such a two-peak scenario, the higher mass peak would be the ι since its mass and width are consistent with those attributed to that state.[22–24]

VI. SPIN-PARITY ANALYSIS

A spin-parity analysis was performed on the events in the $K_S^0K_S^0\pi^0$ mass region from threshold to 1630 MeV/c^2. The analysis follows the Zemach-tensor method[32] by performing maximum-likelihood fits to Dalitz plots in seven mass intervals. Complete details of the analysis method are available in Ref. 30. Fits were carried out on the 6265 events satisfying kinematic fits and cuts, as well as on the 2953 events with the t cut ($t'>0.2$ GeV^2) imposed.

The Dalitz plots were analyzed in a manner which isolated specific regions of the $K_S^0K_S^0\pi^0$ mass spectrum. The data are divided into seven bins: $f_1(1285)$ region, lower, middle, and upper E regions, and three sideband regions. The mass limits and the populations of each bin are shown in Table I. The Dalitz plots for the data without a t' cut are shown in Fig. 9 for the three E regions and the $f_1(1285)$ region. In these plots, each event is plotted twice.

It was shown in the previous section that the $K_S^0K_S^0$ and the $K_S^0\pi^0$ effective mass spectra reveal the presence of the intermediate resonances $K^*(892)$ (in $K_S^0\pi^0$), $a_0(980)$, and $a_2(1320)$ (in $K_S^0K_S^0$). The K^* will appear as bands at m_{13}^2 and $m_{23}^2=0.8$ (GeV/c^2)^2, as is apparent in the upper E region and the two higher sidebands. The constructive interference between the K^* bands causes the overlap region to be enhanced relative to the simple superposition of the bands. The threshold $K_S^0K_S^0$ resonance $a_0(980)$ appears as a diagonal band across the upper edge of the plots, and is seen in the $f_1(1285)$ region, as expected, since the $f_1(1285)$ is known to decay into $a_0\pi$ (Refs. 1, 5, and 7). In the lower and middle E region (the region of

TABLE I. Dalitz-plot-fit region limits and populations.

Region	Mass range (MeV)	Events	Events $t'>0.2$ GeV^2
$f_1(1285)$ region	1260–1300	98	57
Sideband 1	1300–1390	138	81
Lower E region	1390–1430	155	101
Middle E region	1430–1460	131	82
Upper E region	1460–1530	350	182
Sideband 2	1530–1580	205	83
Sideband 3	1580–1630	286	111

the K^*K threshold) the K^* and $a_0(980)$ bands overlap, and thus the apparent bands could be due to the $a_0\pi$ and/or the K^*K final state.

Zemach tensors

The tensors were constructed according to the isobar formalism, in which the decay is assumed to proceed through the formation of an intermediate, two-body resonance. The spin of this resonance is represented by a covariant tensor which has zero timelike components when evaluated in the two-body rest frame. The spacelike part of this tensor is used to represent the helicity of the two-body resonance in the three-body rest frame.

The formation of resonances results in an increased population density in the region of the mass of the resonance. Thus, the energy dependence of the population density includes a parametrization of this resonance structure. Two such resonances are expected in the analysis region—the $K^*(892)$ and the $a_0(980)$.

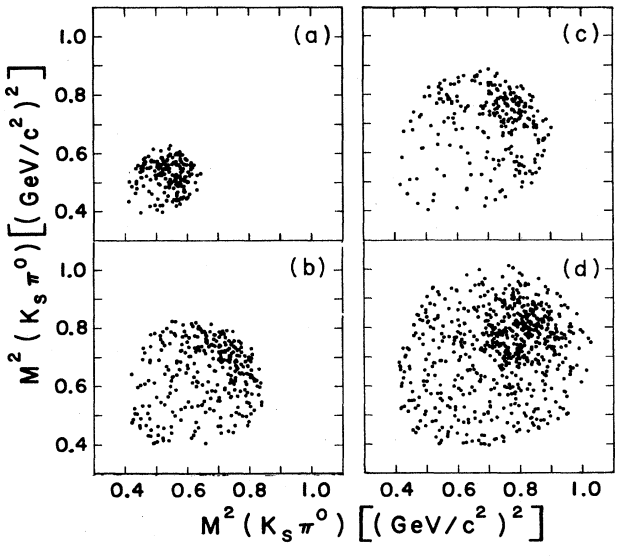

FIG. 9. Dalitz plots for the data without a t' cut, in (a) the $f_1(1285)$ region, (b) the lower E region, (c) the middle E region, and (d) the upper E region. Each event is entered twice in these plots.

The K^* is parametrized by a Breit-Wigner resonance function. The $a_0(980)$ is known to decay into both the $\eta\pi$ and $K\bar{K}$ final states. In fitting both decay channels, the resonance has been parametrized by a coupled-channel resonance form given by Flatté:[31]

$$
\begin{aligned}
F_F &= \frac{m_{a_0}\sqrt{\Gamma_0\Gamma_i}}{m_{a_0}^2 - m_{12}^2 - i m_{a_0}(\Gamma_{\pi\eta}+\Gamma_{K\bar{K}})} , \\
\Gamma_{\pi\eta} &= g_\eta q_\eta , \\
\Gamma_{K\bar{K}} &= g_K q_K , \\
\Gamma_i &= \text{either } \Gamma_{\pi\eta} \text{ or } \Gamma_{K\bar{K}} .
\end{aligned}
\tag{3}
$$

[This form is referred to as a δ parametrization, in reference to the old name for the $a_0(980)$.] The factor q_η is the breakup momentum of m_{12} into the $\eta\pi$ final state and q_K is the breakup momentum into the $K\bar{K}$ final state. The a_0 resonance mass is given by m_{a_0}. The coupling strength to each decay channel is represented by the constants g_η and g_K. $\Gamma_{\pi\eta}$ and $\Gamma_{K\bar{K}}$ are the partial decay widths into each decay channel. The factor Γ_0 is the incoming width. Defining q_0 to be the breakup momentum of the $\eta\pi$ system when $m_{\eta\pi}=m_{a_0}$, Γ_0 is then defined as $\Gamma_0=q_0 g_\eta$. For the fits presented here, the ratio g_K/g_η is taken to be 1.5—the value predicted by SU(3) calculations.[33] The resonance mass m_{a_0} is 983 MeV/c^2, as determined from observation of this state in the $\eta\pi$ decay channel.

A more rigorous treatment of the δ parametrization[34] involves expressing the term m_{a_0} (observed in the $K\bar{K}$ channel) as a function of the coupling strength ratio g_K/g_η. A parametrization of this form was also tried and was found to give essentially the same results.

The tensors included in the Dalitz plot fits are given in Table II. Spins of $J=1$ and 0 are allowed, involving therefore tensors of rank 1 (a three-vector) and rank 0 (a scalar). The angular momentum L between the K^* and K_S^0 (or between the a_0 and the π^0) is allowed to be 0 (S wave) or 1 (P wave) only. There have been no previous experimental results which have indicated the presence of resonance states coupling to the $K^*K(D)$ or $a_0\pi(D)$ ($L=2$) channels in $K\bar{K}\pi$ from threshold through the E region. Higher-L states were therefore not included in the fits.

TABLE II. Tensors describing the spin-parity and decay-channel combinations alllowed in the fits to the Dalitz plots.

Decay channel (L)	Spin parity	Amplitude[a]
Background		constant
$a_0\pi(S)$	0^-	(F_F)[b]
$a_0\pi(P)$	1^+	$(F_F)(\mathbf{p}_3)$
$K^*K(S)$	1^+	$[F_{BW}(13)(\mathbf{t}_{13})+F_{BW}(23)(\mathbf{t}_{23})]$[c,d]
$K^*K(P)$	0^-	$[F_{BW}(13)(\mathbf{t}_{13}\cdot\mathbf{p}_2)F_{BW}(23)(\mathbf{t}_{23}\cdot\mathbf{p}_1)]$

[a]Subscripts 1 and 2 refer to variables of the K_S's, subscript 3 refers to variables of the π^0.
[b]F_F denotes the Flatté parametrization of the a_0.
[c]F_{BW} refers to the Breit-Wigner resonance form of the K^*.
[d]$\mathbf{t}_{ij}$ is the three-vector part of the covariant form of the vector $\mathbf{p}_j-\mathbf{p}_i$.

Each of the functions in Table II represents a $K_S^0K_S^0\pi^0$ state of a specific spin-parity and decay channel, referred to here as $A^i_{J^P}$, i indicating the decay channel. Each spin-parity amplitude A_{J^P} is the sum of the decay channels of like spin, and the intensity is the absolute square of this sum (where it is assumed there are two decay channels a and b):

$$|A_{J^P}|^2=\left|\sum_i \alpha_i A^i_{J^P}\right|^2$$
$$=\alpha_a^2|A^a_{J^P}|^2+\alpha_b^2|A^b_{J^P}|^2$$
$$+\alpha_a\alpha_b\cos\delta_{ab}(|A^{a*}_{J^P}A^b_{J^P}|+|A^{b*}_{J^P}A^a_{J^P}|)\ . \quad (4)$$

Here α_i are the constants which determine the contribution from each decay channel. In Eq. (4), the final term represents the interference between the decay channels of like spin, where the coherence is a variable of the fit, here indicated by the parameter δ_{ab}. Each of the terms in the absolute value in Eq. (4) is normalized over the available phase space ρ and is acceptance corrected:

$$|A^i_{J^P}|^2=\frac{|A^{i\prime}_{J^P}|^2}{\int W(\rho)|A^{i\prime}_{J^P}(\rho)|^2d\rho}\ , \quad (5)$$

where the primes indicate the unnormalized function and $W(\rho)$ is the acceptance function.

The overall intensity I at point (m^2_{13},m^2_{23}) is then a sum over all spin-parities,

$$I(m^2_{13},m^2_{23})=\frac{\sum_{J^P}|A_{J^P}(m^2_{13},m^2_{23})|^2}{\sum_{ij}(\alpha_i\alpha_j)}\ , \quad (6)$$

in which the normalization factor $\sum_{ij}(\alpha_i\alpha_j)$ is included. The likelihood $\mathcal{L}$ for the entire plot is the product of the intensities given by Eq. (6) calculated at each point in the plot (for N points in the plot):

$$\mathcal{L}=\prod_{j=1}^{N} I_i\ . \quad (7)$$

In fitting, the program MINUIT is used to maximize the logarithm of the likelihood for the plot by adjusting the five values α_i and the two interference angles δ_{0^-} and δ_{1^+}, where the subscript indicates the interference between the decay channels of the 0^- and 1^+ waves. The logarithm of the likelihood, $\ln\mathcal{L}$, for a plot of N events is then

$$\ln\mathcal{L}=\sum_{n=1}^{N}\ln\frac{\sum_{J^P}|A_{J^P}|^2}{\sum_{ij}|\alpha_i\alpha_j|}\ . \quad (8)$$

To compare the fit results across the entire fit region, each parameter is normalized by $(\sum_{ij}\alpha_i\alpha_j)$ and multiplied by the number of events per 10 MeV in the fit region to compensate for the uneven bin sizes. The intensity of a spin-parity decay-channel combination η_i is the normalized square of the parameter multiplying it:

$$\eta_i=\left[\frac{\alpha_i^2}{\sum_{ij}\alpha_i\alpha_j}\right]\frac{N}{w}\ , \quad (9)$$

where w is the width of the bin . The intensity of the spin-parity state η_{J^P} includes contributions from both decays (a and b) as well as the interference factor:

$$\eta_{J^P}=\left[\frac{\alpha_a^2+\alpha_b^2+2\alpha_a\alpha_b\cos\delta_{ab}}{\sum_{ij}\alpha_i\alpha_j}\right]\frac{N}{w}\ . \quad (10)$$

The values η_i and η_{J^P} are those that are plotted when summarizing the results of the fits.

To test the method and to fully understand the statistical limitations inherent in our data, Monte Carlo samples were generated (with acceptance effects included) with the same number of events as are present in the data with several combinations of decay-channel contributions. Plots generated with combinations of $K^*K(S)$ and $K^*K(P)$ waves lead to fits with the generated values of the parameters in all three E regions. On the other hand, fits to plots generated with equal contributions from the $K^*K(S)$, $a_0\pi(S)$, and background waves led to fits which tended to have too small of a contribution from the generated $a_0\pi(S)$ wave in the lower and middle E regions. This effect was found to be due to statistical limitations.

It was found that twice as many events were needed in the lower E region, and 10 times as many events were needed in the middle E region to consistently reproduce the generated values of the parameters. In the upper E region, plots generated with the same number of events as the data successfully reproduced the initial parameters, reflecting the movement of the K^* band away from the $a_0(980)$ region.

The error analysis for the fits in the E regions was carefully done to take into account the statistical limitations. Monte Carlo acceptance-attenuated plots were generated with the fitted parameters and the same number of events as in the data. For each E region, 100 Monte Carlo samples were generated and fitted. A distribution was produced for each variable from the Monte Carlo fit results. The error is determined from the assumption that 68% of the fits will fall within $\pm\sigma$ of the central value. The σ thus derived is shown as the error bars in the E region in Figs. 10 and 11. (Outside of the E region, the error bars shown were calculated from the covariance matrix of the fit which generally produced smaller errors.) In cases (lower and middle E regions of the t-cut data) where the error bars are asymmetric, the result of the original fit does not correspond to the center of the Monte Carlo distribution for that parameter. The horizontal error bars on each point indicate the extent of the fit region in $K_S^0K_S^0\pi^0$ mass.

Results of fits to data without a t' cut are shown in Fig. 10. The fits for the $f_1(1285)$ region indicate a large contribution from the 1^{++} wave, consistent with production of the $f_1(1285)$. The suggestion of a sizable contribution from the 0^{-+} wave in this region is interesting in light of possible $\eta(1280)$ production, but while the contribution from 0^{-+} is $\frac{2}{3}$ that of the 1^{++} wave, the large uncertainty in the 0^{-+} intensity makes definite conclusions difficult. Both the 0^{-+} and 1^{++} contributions in the $f_1(1285)$ region are observed to be mostly $a_0\pi$.

In the E regions the 1^{++} wave rises quickly to a steady value, primarily due to the $K^*K(S)$ wave, above the lower E region. In the lower E region the 1^{++} wave is entirely $a_0\pi(P)$. The total 1^{++} wave intensity is consistent with a nonresonant rise across the E region.

Results of fits to the data with the cut $t' > 0.2$ GeV^2 are

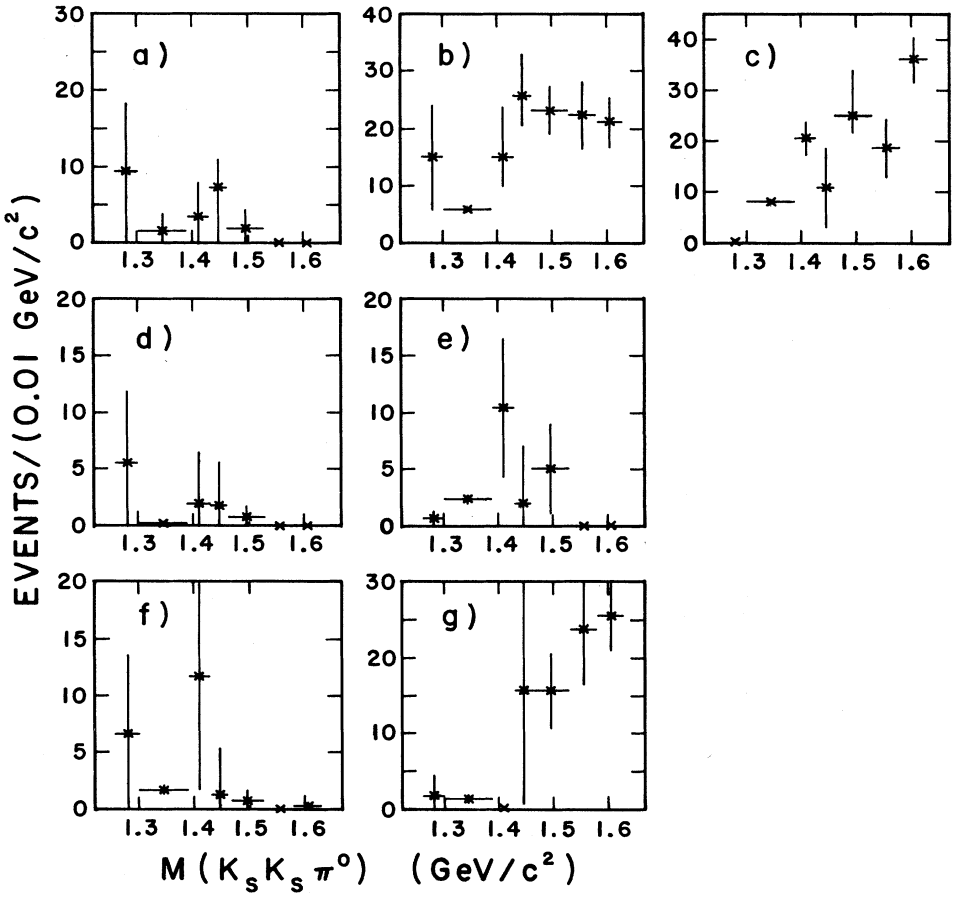

FIG. 10. Dalitz-plot fits to the data without a t' cut; intensities of the total (a) 0^{-+}, (b) 1^{++}, and (c) background as a function of $K_SK_S\pi^0$ mass. The contributions from the decay channels are shown in (d) $0^{-+}\delta\pi(S)$, (e) $0^{-+}K^*K(P)$, (f) $1^{++}\delta\pi(P)$, and (g) $1^{++}K^*K(S)$.

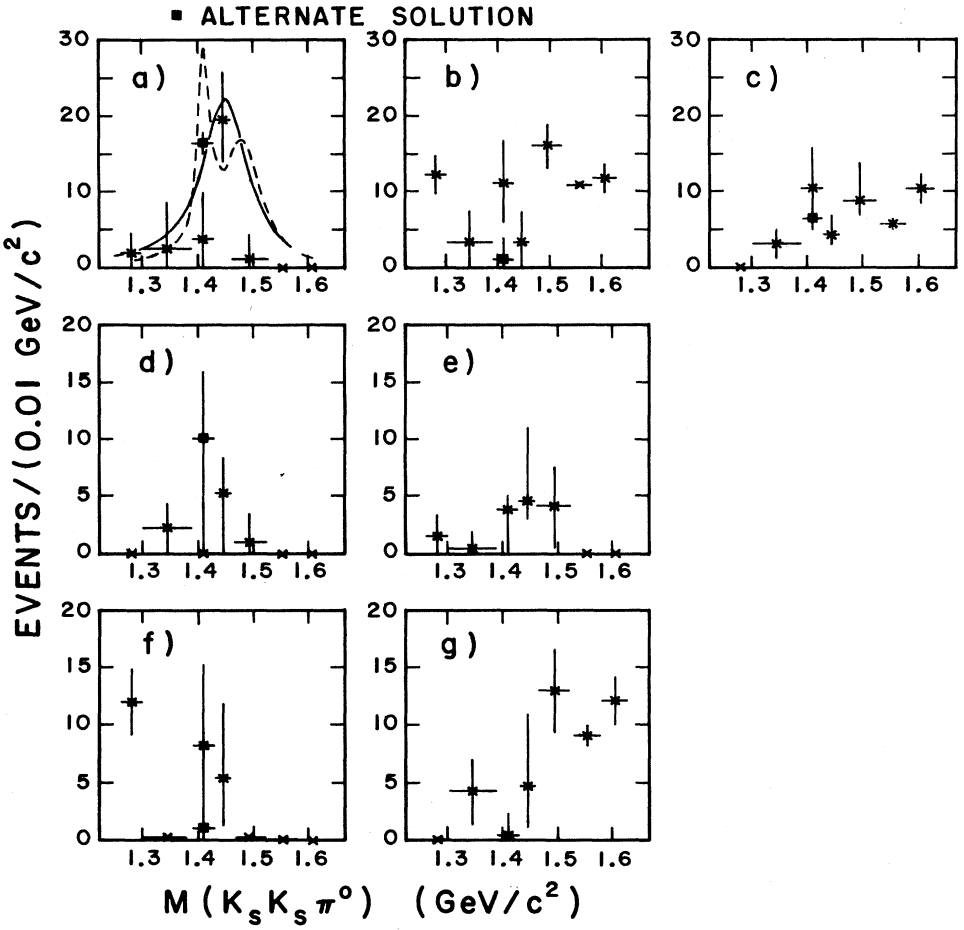

FIG. 11. Dalitz-plot fits to the data with a t' cut; intensities of the toal (a) 0^{-+}, (b) 1^{++}, and (c) background as a function of $K_SK_S\pi^0$ mass. The solid superimposed curve in (a) represents the single-peak fit to the effective-mass distribution in the E region. The dashed curve in (a) represents the two-peak fit to this region. The "alternate solution" is explained in the text. The contributions from the decay channels are shown in (d) $0^{-+}\delta\pi(S)$, (e) $0^{-+}K^*K(P)$, (f) $1^{++}\delta\pi(P)$, and (g) $1^{++}K^*K(S)$.

shown in Fig. 11. The t' cut enhances the 0^{-+} wave relative to the 1^{++} in each region except the $f_1(1285)$ and those sidebands above the E. The $f_1(1285)$ region is nearly 100% 1^{++} $a_0\pi(P)$ wave in this fit. In the E region the overall 1^{++} wave [Fig. 11(b)] rises smoothly from K^*K threshold as observed in the uncut data.

TABLE III. Decrease observed in the logarithmic likelihood when individual waves are removed from fits (t'-cut data).

Wave removed	Decrease in $\ln\mathcal{L}$ by region		
	Lower E	Middle E	Upper E
$K^*K(P)$	2.5	7.3	1.7
$K^*K(S)$	0.2	0.9	24.5
$a_0\pi(S)$	0.3	1.1	1.1
$a_0\pi(P)$	0.0	1.2	0.6
$a_0\pi(S$ and $P)$	6.2	4.6	1.1
$K^*K(S$ and $P)$	2.6	12.0	41.6
	$\ln\mathcal{L}$ of the best fit		
None	633.7	503.4	921.1

Table III shows the change in likelihood resulting from the removal of various waves from the fit in the E regions. It is clear from this table that an $a_0\pi$ contribution is needed to fit these regions. However, the fit cannot distinguish between the $1^{++}a_0\pi(P)$ wave and the $0^{-+}a_0\pi(S)$ wave contribution with the low available statistics. The ambiguity between the two $a_0\pi$ waves was also apparent in the Monte Carlo study of the lower E region. In fact, during the systematic study of the statistical significance of the fits to the data, an alternate solution was found in the single bin centered at 1410 MeV. This solution, shown in Fig. 11, arises from substituting $a_0\pi(S)$ wave for the $a_0\pi(P)$ wave in the fit.

The peak in the 0^{-+} wave is consistent with the single Breit-Wigner fit to the E region described earlier (particularly with the alternate solution in the lower E region), but is also consistent with the two Breit-Wigner fit when both peaks are assumed to be spin zero. The solid curve [Fig. 11(a)] represents a Breit-Wigner resonance at 1455 MeV/c^2 of width 100 MeV/c^2, corresponding to the

single-peak fit to the E region. The mass and width, combined with the 0^{-+} spin-parity assignment, are consistent with the identification of this peak as the $\iota(1460)$. The dashed curve [Fig. 11(a)] represents the sum of the two Breit-Wigner resonances in the two-peak fit. The one- and two-peak fits appear to be equally consistent with the Dalitz-plot fit results. The sharp rise observed in the 1^{++} intensity [Fig. 11(b)] at about 1500 MeV/c^2 is consistent with the production of $K^*K(S)$ wave background. Thus the Dalitz-plot fits support the conclusion that the structure in the E region is due to the production of one or two pseudoscalar resonances in the presence of a rapidly rising 1^{++} (mostly K^*K) background.

VII. SUMMARY AND CONCLUSIONS

The $K_S^0K_S^0\pi^0$ final state in the reaction

$$\pi^-p\rightarrow K_S^0K_S^0\pi^0n$$

has been investigated. The $K_S^0K_S^0\pi^0$ effective-mass distribution from this event sample contains evidence of $f_1(1285)$ production as well as a broad enhancement over a quickly rising background in the 1400–1500-MeV region. No statistically significant enhancements were observed at higher mass.

The two-body effective-mass distributions ($K_S^0K_S^0$ and $K_S^0\pi^0$) indicate production of $a_0(980)$, $a_2(1320)$, and $K^*(892)$ resonances. The $a_0(980)$ is observed as a threshold peak in the $K_S^0K_S^0$ effective-mass distribution.

The $K_S^0K_S^0\pi^0$ system is produced peripherally. In the region below 1.5 GeV/c^2, the events are produced with a much flatter t distribution than those above this mass. A cut on the momentum transfer, $-t'>0.2$ GeV^2 was observed to enhance the peak seen in the E region. In fitting the $K_S^0K_S^0\pi^0$ effective-mass spectrum with two or three Breit-Wigner resonances and a background, two solutions were found. In both solutions, a peak in the $f_1(1285)$ region was observed with a mass and width of 1282 and 18 MeV/c^2, respectively, consistent with $f_1(1285)$ production. In the first solution, the enhancement in the E region yielded a Breit-Wigner mass of 1453 MeV/c^2 and a width of 100 MeV/c^2. The second solution had two Breit-Wigner fits in the E region with masses of 1412 and 1475 MeV/c^2 and widths of 19 and 51 MeV/c^2. (Somewhat broader fits resulted if the enhancements were assumed to have spin 1.) The two-peak fit in the E region has a χ^2 probability of 28.8% which is somewhat preferred over the single-peak fit (probability of 2.7%).

Fits to the Dalitz plots at various masses are characterized by an $a_0\pi$ 1^{++} peak in the $f_1(1285)$ region and a sharp rise of the 1^{++} K^*K S wave to a steady value above the K^*K production threshold. The 0^{-+} intensity shows evidence of peaking in the E region and this peaking is enhanced when selecting on larger t'. Both the single Breit-Wigner fit and the two Breit-Wigner fit to the E region are found to be consistent with the peak observed in the 0^{-+} intensity. These conclusions are even better supported by an "alternate solution" found in the lower E region.

The results on the $f_1(1285)$ region—spin-parity, decay channel, mass, and width—all agree with the parameters of the $f_1(1285)$, in agreement with observations of previous experiments.[1,5,7]

An important observation of this experiment is that the peak observed in the E region is different than that seen in lower-energy peripheral hadroproduction experiments and is consistent in mass, width, and spin-parity with the $\iota(1460)$ observed in J/ψ radiative decay. The $\eta(1420)$ enhancement observed in these other hadroproduction experiments[1,5] is significantly lower in mass and narrower than the structure observed here. These differences are due most likely to a combination of the fact that our experiment was done at higher energy, thus possibly involving different production mechanism combinations, and perhaps more importantly, that our experiment excludes states with $C=-1$ and the interference effects caused by them.

If the $\iota(1460)$ is considered to be an admixture of $q\bar{q}$ and gluonic components,[35–37] its production in this experiment might be expected to occur through the $q\bar{q}$ component although hadronic production of pure gluonic states is certainly possible.[38] Also, because the initial π^-p state contains only u and d quarks, the observed signal might further be expected to be dominated by the $u\bar{u}$ and $d\bar{d}$ portions of the wave function.

It is possible that the $\eta(1420)$ and the $\iota(1460)$ are the same state, whose observed mass and width have been affected by a mass- and energy-dependent production mechanism. In this case, our single Breit-Wigner fit in the E region is the correct fit. However, if there are two separate states in the E region (consistent with our second fit to the mass spectrum), slightly different conclusions can be drawn. The narrow, lower-mass enhancement would be the $\eta(1420)$. Its mass, width, and spin parity are consistent with this identification. The higher-mass peak would then be the ι. We note however that the mass of this peak is, in this case, somewhat higher (by $\sim$20 MeV/c^2) than most observations of the ι mass.

ACKNOWLEDGMENTS

We would like to acknowledge the assistance of Ronald Erichsen, the MPS technicians, and the AGS staff in the execution of this experiment. This work was supported by the National Science Foundation and the Department of Energy.

*Present address: AT&T Bell Laboratories, Whippany, NJ 07981.

†Present address: Northern Illinois University, DeKalb, IL 60115.

‡Present address: Fermi National Accelerator Laboratory, Batavia, IL 60510.

§Present address: Florida State University, Tallahassee, FL 32306.

**Present address: Hughes Aircraft Corp., Los Angeles, CA.
[1]S. U. Chung *et al.*, Phys. Rev. Lett. **55**, 779 (1985); S. U. Chung, in *Proceedings of the XXIII International Conference on High Energy Physics,* Berkeley, California, 1986, edited by S. C. Loken (World Scientific, Singapore, 1987), Vol. I, p. 725; A. Birman *et al.*, Phys. Rev. Lett. **61**, 1557 (1988).
[2]C. Dionisi *et al.*, Nucl. Phys. **B169**, 1 (1980).
[3]O. I. Dahl *et al.*, Phys. Rev. **163**, 1377 (1967).
[4]N. Stanton *et al.*, Phys. Rev. Lett. **42**, 346 (1979).
[5]A. Ando *et al.*, Phys. Rev. Lett. **57**, 1296 (1986).
[6]D. F. Reeves *et al.*, Phys. Rev. D **34**, 1960 (1986).
[7]T. Armstrong *et al.*, Phys. Lett. **146B**, 273 (1984).
[8]T. Armstrong *et al.*, Z. Phys. C **34**, 23 (1987).
[9]T. A. Armstrong *et al.*, in *Glueballs, Hybrids and Exotic Hadrons,* proceedings of the BNL Workshop, Upton, New York, 1988, edited by S. U. Chung (AIP Conf. Proc. No. 185) (AIP, New York, 1989), p. 340.
[10]R. Landua *et al.*, in *Glueballs, Hybrids and Exotic Hadrons* (Ref. 9), p. 246.
[11]H. Aihara *et al.*, Phys. Rev. Lett. **57**, 51 (1986).
[12]H. Aihara *et al.*, Phys. Rev. Lett. **57**, 2500 (1986).
[13]H. Aihara *et al.*, Phys. Rev. D **38**, 1 (1988).
[14]G. Gidal *et al.*, Phys. Rev. Lett. **59**, 2012 (1987).
[15]G. Gidal *et al.*, Phys. Rev. Lett. **59**, 2016 (1987).
[16]W. Bartel *et al.*, in *Proceedings of the International Europhysics Conference on High Energy Physics,* Uppsala, Sweden, 1987, edited by O. Botner (European Physical Society, Geneva, Switzerland, 1987).
[17]J. J. Becker *et al.*, Phys. Rev. Lett. **59**, 186 (1987).
[18]Ph. Gavillet *et al.*, Z. Phys. C **16**, 119 (1982).
[19]D. Aston *et al.*, Phys. Lett. B **201**, 573 (1988).
[20]S. Blessing *et al.*, in *Glueballs, Hybrids and Exotic Hadrons* (Ref. 9), p. 363.
[21]P. Baillon *et al.*, Nuovo Cimento **50A**, 393 (1967).
[22]D. L. Scharre *et al.*, Phys. Lett. **97B**, 329 (1980).
[23]C. Edwards *et al.*, Phys. Rev. Lett. **49**, 259 (1982).
[24]J. Perrier, in *Physics in Collision 4,* proceedings of the Fourth International Conference, Santa Cruz, California, 1984, edited by A. Seiden (Editions Frontières, Gif-sur-Yvette, France, 1983), p. 145.
[25]M. G. Rath *et al.*, Phys. Rev. Lett. **61**, 802 (1988).
[26]N. M. Cason *et al.*, in *Glueballs, Hybrids and Exotic Hadrons* (Ref. 9), p. 334.
[27]S. Eiseman *et al.*, Nucl. Instrum. Methods **217**, 140 (1983).
[28]A. Etkin *et al.*, Brookhaven National Laboratory report, 1983 (unpublished).
[29]A. E. Baumbaugh *et al.*, Nucl. Instrum. Methods **197**, 297 (1982).
[30]M. G. Rath, Ph.D. thesis, University of Notre Dame, 1988.
[31]S. M. Flatté, Phys. Lett. **63B**, 224 (1976).
[32]C. Zemach, Phys. Rev. **133**, B1201 (1964).
[33]D. F. Reeves, Ph.D. thesis, Florida State University, Report No. FSU-HEP-850801, 1985.
[34]S. D. Protopopescu, in *Strong Interactions and Gauge Theories,* proceedings of the XXIst Rencontre de Moriond, Les Arcs, France, 1986, edited by J. Tran Thanh Van (Editons Frontières, Gif-sur-Yvette, France, 1986).
[35]S. Meshkov, W. F. Palmer, and S. S. Pinsky, in *Proceedings of the Salt Lake City Meeting,* Annual Meeting of the Division of Particles and Fields of the APS, Salt Lake City, Utah, 1987, edited by C. DeTar and J. Ball (World Scientific, Singapore, 1987), p. 520.
[36]M. S. Chanowitz, Phys. Lett. **164B**, 379 (1985).
[37]B. Bagchi and S. Basu, Mod. Phys. Lett. A **3**, 623 (1988).
[38]R. S. Longacre, in *Glueballs, Hybrids and Exotic Hadrons* (Ref. 9), p. 670.